NJC

Check for updates

A new water stable zinc metal organic framework as an electrode material for hydrazine sensing†

Manzar Sohail, [ID] *[a] Muhammad Altaf, [ID] [a] Nadeem Baig,[b] Rabia Jamil,[c] Muhammad Sher[c] and Atif Fazal[d]

Metal–organic frameworks (MOFs) are an emerging class of materials exhibiting high surface areas, controlled pore sizes, open metal sites and organic linkers. Utilizing MOFs as direct electrode materials for electrochemical sensing can offer inherent advantages such as containing a sensing element and a redox mediator in a single molecule; however, the direct use of MOFs as electrode materials is hindered because of their insulating nature and less stability in an aqueous medium. In this study, a new water stable Zn-MOF was synthesized and used directly as an electrode material. The Zn-MOF possesses good ability to electrocatalyze the hydrazine oxidation reaction. The Zn-MOF's inherent poor conductivity was overcome by including a hydrophobic electrolyte, tetrakis(4-chlorophenyl)borate tetradodecylammonium salt (ETH 500), during the fabrication of the Zn-MOF membrane. After coating a thin film of the nafion-ETH500 supported Zn-MOF over a glassy carbon electrode (GCE), the response for hydrazine oxidation was substantially improved. Linear sweep voltammetry (LSV) demonstrated a wide linear range from 20 to 350 µM (R^2 = 0.9922) for hydrazine. A detection limit of 2 µM (n = 3) was observed. The electrochemical behavior of the ZnMOF/ETH500/nafion modified GCE revealed that MOFs have a promising future as electrode materials for direct electrochemical sensing.

Introduction

The study of metal organic frameworks (MOFs) is currently an interdisciplinary research area and covers the chemical, biological and physical sciences fields (CO_2 capture, gas storage, gas separation, magnetism, ion exchange, catalysis, sensors and luminescence).[1–4] The reticular chemistry of MOFs has been explored intensively over the last two decades. The most appealing feature of MOF chemistry is the beauty of their architecture based on the self-assembly of metal ions with bridging organic linkers. It is a well-known fact that there is a close relationship between the properties of MOFs and their topology/solid state structures. It is a major challenge for researchers to synthesize new MOFs with desired properties and predesigned structures.[5–10] The rational design of linkers and suitable metal centers has made it possible to synthesize new MOFs with a particular structural topology during the last ten years. The unique features of MOFs are their receptivity and responsiveness toward guest molecules, resulting in reversible changes in their physical, optical and chemical properties. Controllable pore sizes, high accessible open metal sites and ordered crystalline structures are added advantages of MOFs. MOFs can be tuned to obtain the desired response from this unique host–guest interaction paving the way to a diverse range of applications including catalysis, carbon capture, separation membranes, drug delivery and sensing. Electrochemical sensing is an area of high demand research because of the attractive advantages it offers over lab based analytical techniques including low cost, point of care analysis, less time and ease of use.[11] However, the direct use of MOFs as electrode materials for electrochemical sensing is in its infancy.[12,13] MOFs possess well-defined pore sizes and pore volumes which can provide a confinement effect for the guest molecules. Furthermore, the selectivity of the MOFs towards guest molecules could arise from the selective H-bonding & van der Waals interactions, π–π interactions and open metal sites.[14,15]

Electrochemical sensors are in general composed of a polymer matrix containing an analyte recognition element (ionophore or enzyme) and a redox mediator for charge transfer between the analyte, sensing element and electrode surface. All solid state electrochemical sensors (SSEs) offer a lot of advantages over liquid junction electrodes. Usually a redox mediator is used as an inner

[a] *Center of Research Excellence in Nanotechnology (CENT),*
King Fahd University of Petroleum and Minerals, Dhahran 31261, Saudi Arabia.
E-mail: manzarsohail@kfupm.edu.sa; Tel: +966 13860 8367
[b] *Chemistry Department, King Fahd University of Petroleum and Minerals,*
Dhahran 31261, Saudi Arabia
[c] *Department of Chemistry, Allama Iqbal Open University, Islamabad, Pakistan*
[d] *Center of Research Excellence in Petroleum Refining and Petrochemicals*
(CoRE-PRP), King Fahd University of Petroleum and Minerals, Dhahran, 31261,
Saudi Arabia

This journal is © The Royal Society of Chemistry and the Centre National de la Recherche Scientifique 2018

layer for charge transfer between the electrode and the outer polymer layer in SSEs. Well known problems in the membrane based SSEs are the leaching of dissolved mediators or diminished electrochemical accessibility of redox species covalently attached to polymeric membranes.[16–18] MOFs can be compared with redox polymers used in the fabrication of electrochemical sensors.[19] However, a balance between redox capacity and resistance is required to acquire the desired selectivity of MOFs as electrode materials.[20] The mechanical properties of MOFs are also important for their use as an electrode material. In principle, a rationally designed MOF can offer the possibility of containing a redox mediator, a polymer matrix and a sensing element in a single molecule.[18] However, some challenges need to be addressed before MOFs can be fully inculcated in the SSE field. These challenges include the synthesis of redox active MOFs,[15] the high resistance/ poor conductivity of MOFs and the poor stability of MOFs in an aqueous medium.[12,15] Over the last 5 years, several new MOFs have been reported for optical sensing,[15,21–24] proton conduction[25,26] and electrochemical sensing of metal ions.[14]

On the other hand, hydrazine and its derivatives are getting attention in various fields including agriculture, aerospace, fuels, catalysis, and military applications.[27,28] Hydrazine is also used as an intermediate in many pharmaceutical, antioxidant, and emulsifier products, and also acts as a corrosion inhibitor in industrial boilers. Despite its huge number of applications, hydrazine is a hazardous material and considered as carcinogenic for humans.[28,29] In animals, it was observed that hydrazine could affect their spinal cord, liver, DNA, brain, and kidneys, and might cause injury to the lungs.[28,30] Different analytical methods based on chromatography,[31] luminescence,[32] spectroscopic[33] and electrochemical[34] sensing have been utilized for hydrazine sensing. The electrochemical methods are acquiring high consideration due to their advantages stated above. Recently, a few composite materials comprising MOFs and conducting materials or nanostructures have been reported for electrochemical sensing of glucose,[35] dopamine,[36] catechol,[37] hydrazine[38] and cadmium ions.[39] The direct utilization of MOFs as sensing platforms is gaining increasing attention. In recent years, MOFs have been being reported as biomimetic systems for the sensing of glucose,[40] catechol[37] and hydrogen peroxide.[41] However, the direct utilization of MOFs as standalone electrode materials is still in its infancy.

Herein, we report a new water stable Zn-MOF which can be used as an electrode material for hydrazine sensing. A mixed ligand approach, with a flexible chain and rigid N-donor linker, was used for Zn-MOF synthesis. To mitigate the high resistance, a concept of using ETH 500 was borrowed from the all solid state ion selective electrode configuration.

Experimental

Instrumentation and materials

An Autolab PGSTAT-101 electrochemical workstation (Eco-Chemie, Metrohm, Autolab, Netherlands) was used for voltammetric measurements with a standard three-electrode system. The working electrode was the ZnMOF/ETH500/nafion modified glassy carbon electrode (GCE). The counter electrode was a platinum wire and the reference electrode was Ag/AgCl/3 M KCl. Zn-MOF single crystal X-ray diffraction data were collected on an Oxford Diffraction Gemini CCD diffractometer employing Cu Kα radiation (1.54180 Å). Elemental analyses were performed on a Perkin Elmer Series 11 (CHNS/O), Analyzer 2400. The solid state FT-IR spectra of the ligands and their Zn(II) MOF were recorded on a Perkin-Elmer FT-IR 180 spectrophotometer or NICOLET 6700 FT-IR using KBr pellets over the range of 4000–400 cm^{-1}. ^{1}H and ^{13}C NMR spectra were recorded on a LAMBDA 500 spectrophotometer operating at 500.01, 125.65 and 200.0 MHz, respectively; corresponding to a magnetic field of 11.74 T. Powder X-ray diffraction (PXRD) analysis was carried out on a 3040/60 X'Pert PRO X-ray diffractometer (Netherlands). (Further details of the apparatus are in the ESI†).

Zn(NO$_3$)$_2$·6H$_2$O, terephthalic acid (bdc), and all the reagents and solvents were purchased from Aldrich. These chemicals were used without further purification, unless otherwise mentioned.

Synthesis of *N,N'*-bis(pyridin-3-ylmethyl)cyclohexane-1,4-diamine

Following the scheme in eqn (1), 3-pyridinecarboxaldehyde (5 g, 46.68 mmol) and (1r,4r)-cyclohexane-1,4-diamine (5.33 g, 46.68 mmol) were added in ethanol (30 mL). Then, triethylamine (7.08 g, 70.02 mmol) was added slowly and refluxed for 4 h. The reaction mixture was cooled and then portion wise addition of NaBH$_4$ (4.41 g, 116.7 mmol) was carried out and the reaction contents were stirred overnight at room temperature. (Detailed procedure is in the ESI†).

(1)
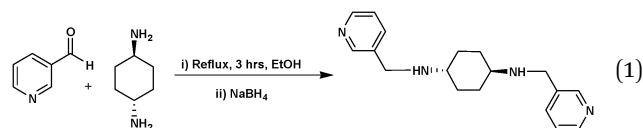
Synthesis of the precursor metal–organic framework (MOF)

Zn(NO$_3$)$_2$·6H$_2$O (0.297 g, 1.0 mmol), *N,N'*-bis(pyridin-3-ylmethylene)-cyclohexane-1,4-diamine (3-bpcda) (0.297 g, 1.0 mmol) and H$_2$bdc (0.172 g, 1.0 mmol) were added in DMF/H$_2$O (10 mL, v/v: 3/1). The reaction mixture was placed in a glass vial and heated at 105 °C for 72 h. Yellow block-shaped crystals were collected and washed with DMF three times (10 mL). The final product was dried in air at room temperature and used for further studies.

Preparation of a ZnMOF/ETH500/nafion GCE

5 wt% of Zn-MOF and 2 wt% of ETH 500 were mixed in 2% nafion solution in THF. The mixture was sonicated for 10 minutes to disperse the Zn-MOF crystals homogeneously. 10 μL of the resulting solution was drop cast twice over a GCE (0.024 cm^2 surface area) and dried in air for 10 minutes. The resulting ZnMOF/ETH500/nafion GCE was used as the working electrode for hydrazine sensing. For PXRD analysis, ZnMOF/ ETH500/nafion was drop cast over fluorine doped tin oxide (FTO) glass.

Results and discussion

Crystal structure of Zn-MOF

The Zn-MOF crystallizes in a triclinic crystal system with a space group $P\bar{1}$. The Zn-MOF features a 2D ring like infinite chain metal–organic framework in which Zn(II) metal centers are interlinked by bdc and 3-bpcda organic linkers as shown in Fig. 1. The X-ray structure reveals that the asymmetric unit of the Zn-MOF consists of a Zn(II) cation, two water molecules and half a unit of each 3-bpcda and bdc linker (Fig. 1S, ESI†). In this structure each Zn(II) atom is surrounded by two nitrogen donor atoms of pyridyl from a pair of 3-bpcda linkers in *trans*-arrangement, two oxygen donor atoms from two separate bdc linkers and two oxygen atoms from coordinated water molecules to display a octahedral geometry. The Zn(II) atom in a 2D chain is residing on a crystallographic inversion center. The Zn(II) metal center in this structure adopts a distorted octahedral geometry with two water molecules on the axial position [Zn–Ow = 2.131(1) Å]. The equatorial position is occupied by two N donors of 3-bpcda and two oxygen atoms of bdc linkers [Zn–N = 2.149(1) and Zn–O = 2.106(1) Å]. The bdc linker connects the Zn(II) atoms of the zigzag infinite 1D cationic chains into a stacked 2D framework (Fig. 2 and Fig. 2S and 3S, ESI†).

Electrochemical behavior of the ZnMOF/ETH500/ nafion-modified electrode for hydrazine

The electrochemical behavior of hydrazine was investigated at the bare and the modified GCE surface. The cyclic voltammo-gram (CV) over a wide potential range (Fig. 5S, ESI†) with the ZnMOF/ETH500/nafion GCE showed a broad oxidation peak for hydrazine with a maximum peak current at a potential (E_p) of 0.276 V. A slow decrease in the oxidation current was noticed. The negative potential sweep showed that no reduction peak was detected indicating that the electrooxidation of hydrazine with the ZnMOF/ETH500/nafion GCE was an irreversible pro-cess, as reported earlier with a platinum electrode.[42] Further electrochemical investigations were carried out with linear scan voltammetry (LSV) carried out in a 0.1 M K_2SO_4 solution and the results are presented in Fig. 3. The bare GCE surface displayed a poor response for 1 mM hydrazine in 0.1 M K_2SO_4 solution. The oxidation peak of hydrazine appeared at
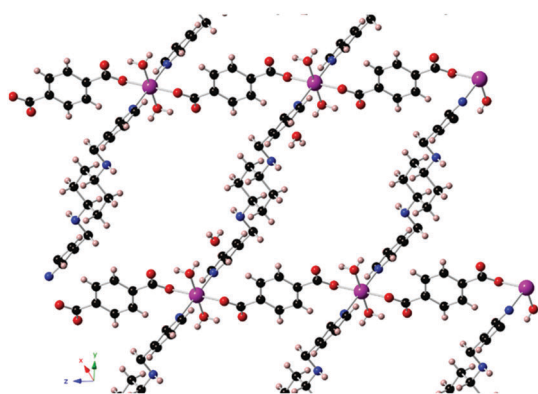

Fig. 1 A view of the crystal structure of the Zn-MOF illustrating the linkage of the Zn(II) centre with organic linkers.
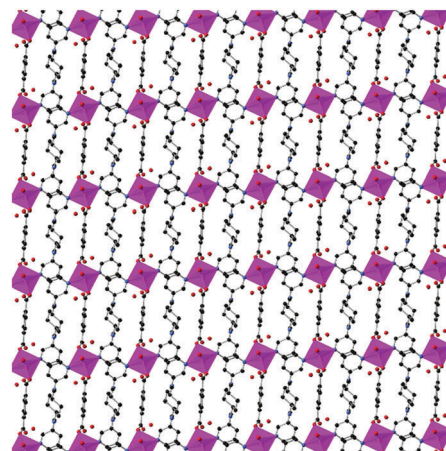

Fig. 2 A view of the 2D framework of the Zn-MOF along the *a*-axis.

0.572 V and the current response was very weak (Fig. 3Aa) for 1 mM of hydrazine. The appearance of a peak at high potential and poor current was an indication of the sluggish electro-chemical behavior of the GCE for hydrazine. After the modifica-tion of the GCE with the ZnMOF/ETH-500/nafion membrane, a strong oxidation peak for hydrazine was observed at E_p 0.276 V (Fig. 3Af). The electrochemical behavior of the ZnMOF/ nafion-modified GCE was measured for 0.350 mM hydrazine. It is evident (Fig. 3Ab) that the current response of the ZnMOF/ nafion-modified GCE (without ETH 500) was also poor with a very small catalytic current, which implies poor conductivity of the ZnMOF/nafion film in the absence of ETH 500. As evident from Fig. 3A and B, the current response was significantly improved with the ZnMOF/ETH500/nafion-modified GCE com-pared to the bare GCE, ZnMOF/nafion or ETH500/nafion films. The shifting of the oxidation peak, to 0.296 V lower compared to the bare GCE, and improvement in oxidation current response may be due to the unique metal organic framework having open metal catalytic sites (Fig. 1 and 2) and specific chemical interactions.[14,41,43] This, in turn, might improve the electro-chemical redox reaction of hydrazine. However, poor charge transfer from the ZnMOF/nafion film was improved with the inclusion of 2 wt% of ETH 500 electrolyte in the membrane. The synergistic effect of the ZnMOF catalysis and the presence of electrolyte overall improved the kinetics of the ZnMOF/ ETH500/nafion modified GCE. Furthermore, the ZnMOF/ ETH500/nafion GCE was investigated for the linear dynamic range of hydrazine.

The linear sweep voltammetry (LSV) curves were recorded for various concentrations of hydrazine in the 0.1 M K_2SO_4 electrolyte and the results are presented in Fig. 4A. The dynamic linear range of the ZnMOF/ETH500/nafion modified GCE was found to be from 22 to 350 μM (Fig. 4B). For this dynamic linear range the linear regression equation is $I_p = 0.2701C_{Hz} + 1.5554$ ($R^2 = 0.9922$), as shown in Fig. 4B. The limit of detection was found to be 2 μM (S/N = 3). These results demonstrated that MOFs could be utilized as direct electrode materials for SSEs and their charge transfer capacity could be enhanced utilizing a simple electrolyte. The presence of organic interferents, diethylene glycol (100 μM) and
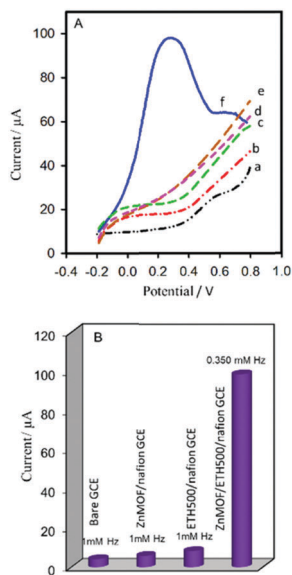
Fig. 3 (A) The LSV response in 0.1 M K_2SO_4 solution, scan rate 50 mV s^{-1}. (a) Bare GCE, (b) ZnMOF/nafion GCE, (c) ETH500/nafion GCE for 1 mM hydrazine, (d) ZnMOF/ETH500/nafion modified GCE for 100 μM ethylene glycol, (e) ZnMOF/ETH500/nafion modified GCE for 100 μM DMF and (f) ZnMOF/ETH500/nafion modified GCE for 0.350 mM hydrazine. (B) Histogram showing the current comparison of the bare, ZnMOF/nafion, ETH500/nafion and ZnMOF/ETH500/nafion modified GCE.

Fig. 4 (A) Linear sweep voltammograms (scan rate 50 mV s^{-1}) recorded using the ZnMOF/ETH500/nafion modified GCE in 0.1 M K_2SO_4 at various concentrations of hydrazine: (a) 0 μM, (b) 22 μM, (c) 50 μM, (d) 100 μM, (e) 150 μM, (f) 175 μM, (g) 225 μM, (h) 250 μM, (i) 275 μM, (j) 300 μM, (k) 325 μM and (l) 350 μM. (B) Linear relationship between peak current (μA) and concentration (μM) of hydrazine (R^2 = 0.9922).

dimethylformamide (100 μM), in the measuring solution had no effect on the response within the potential window tested (Fig. 3Ad and Ae).

The plots of change in E_p (potential for maximum oxidation peak current) with change in hydrazine concentration (Fig. 6SA, ESI†) and change in log of I_p with log of concentration were also plotted (Fig. 6SB, ESI†). It was found that both the oxidation peak current and the corresponding peak potential linearly increased with increasing hydrazine concentration. The rate of variation of E_p with log C_{HZ} is 193 mV (decade C_{hyd})$^{-1}$. Both these plots could also be used for the quantitative determination of hydrazine in the concentration range of 22–350 μM.

Tafel slopes were also plotted between E_p and current (I_p) for different hydrazine concentrations and are presented in Fig. 5A. The Tafel slopes did not change at different concentrations of hydrazine in 0.1 M K_2SO_4, suggesting a concentration independent mechanism for hydrazine oxidation. This was in accordance with reported work [4]. The order of reaction was determined by plotting log I vs. log C_{Hz} (Fig. 5B) at different potential values just below the oxidation peak potential. From the relation, rate = $I = kC^n$, the logarithmic plot of peak current with hydrazine concentration, produced a straight line. The slope of the straight line represents the order of reaction with respect to hydrazine concentration (log I_p = log k + n log C), where I_p is the oxidation peak current, k is the reaction rate constant, C is the bulk concentration and n is the reaction order.[42,44–46] The order of reaction varied from 0.34–0.38, with an average value of 0.36. This order of reaction was close to the work reported earlier for hydrazine determination with a bare platinum electrode.[42,46]

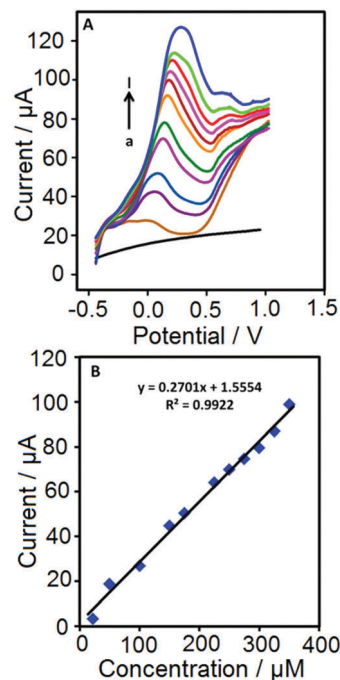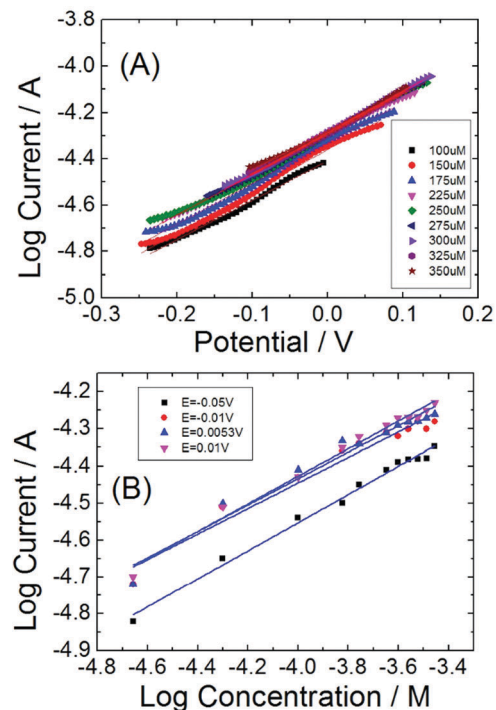

Fig. 5 (A) Influence of hydrazine concentration on the Tafel slopes with the ZnMOF/ETH500/nafion modified GCE in 0.1 M K_2SO_4, scan rate = 50 mV s^{-1}, T = 25 °C. (B) Plots of log I vs. log C_{hyd} at different potential values (below peak potential), 0.1 M K_2SO_4, scan rate = 50 mV s^{-1}, T = 25 °C.
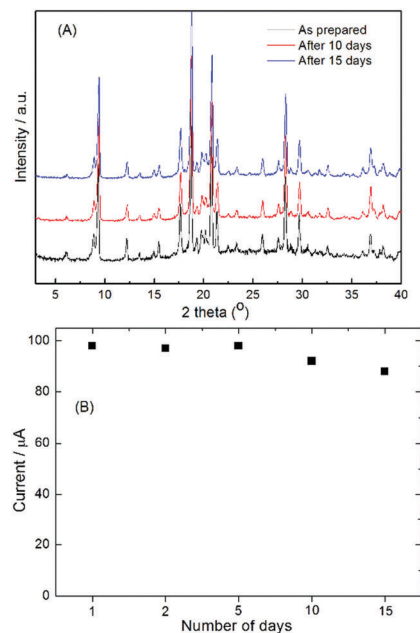
Fig. 6 (A) PXRD patterns of the Zn-MOF soaked in water for different times and (B) oxidation peak current response of the ZnMOF/ETH500/nafion modified GCE for 0.350 mM of hydrazine in 0.1 M K_2SO_4, scan rate = 50 mV s^{-1}, T = 25 °C.

Stability of the Zn-MOF and ZnMOF/ETH500/nafion modified GCE

The Zn-MOF was expected to possess good stability *versus* hydrolysis owing to the fact that it was synthesized in a DMF:water mixture and also the fact that the Zn-MOF crystal structure contained water of crystallinity. The aqueous stability of the Zn-MOF was assessed by soaking the compound in water for two weeks. The PXRD patterns of the as synthesized Zn-MOF and the Zn-MOF soaked in water for up to 15 days are shown in Fig. 6A. Indeed, no noticeable change was observed in the PXRD patterns of the Zn-MOF which represents its excellent aqueous stability. Furthermore, the PXRD patterns of the ZnMOF/ETH500/nafion membrane deposited at the FTO electrode before and after electrochemical experiments also did not show any significant change (Fig. 7S, ESI†).

The results for the recyclability of the response for hydrazine oxidation with the ZnMOF/ETH500/nafion modified GCE are presented in Fig. 6B. Only about 10% loss in the hydrazine oxidation peak current was observed in two weeks. Thus, it was evident that the electrode surface was not affected significantly. Unlike electrochemical sensors for phenols or analytes which have a tendency to polymerize or stick to the surface of the electrode, the products of hydrazine oxidation are only N_2 (gas) and water, thus, the electrode surface was not affected by the analyte or its products.

Conclusions

The results of this study demonstrate that the synthesis of MOFs can be tuned for their direct use as an electrochemical

sensing platform. The ZnMOF/ETH500/nafion GCE demonstrated improved and stable electrochemical activity towards hydrazine. The ZnMOF conductivity on the electrode surface was improved with a well-known electrolyte, ETH500, in ISEs (ion-selective electrodes). The results revealed that the electrochemical behaviour of the GCE was considerably improved after coating with the ZnMOF/ETH500/nafion. This was evident from the shift of the hydrazine oxidation peak towards lower potential and the substantial improvement in the redox current with improved electrode kinetics of the ZnMOF/ETH500/nafion modified GCE. The wide linear range and the good limit of detection demonstrated that MOFs have a promising future in electrochemical sensing due to their unique and attractive structural features. However, a lot of further research is required to synthesize new MOFs with improved selectivity, redox capacity and electrocatalytic behavior.

Conflicts of interest

There are no conflicts to declare.

Acknowledgements

Notes and references

1 R. Banerjee, A. Phan, B. Wang, C. Knobler, H. Furukawa, M. O'Keeffe and O. M. Yaghi, *Science*, 2008, **319**, 939–943.

2 X.-Q. Liang, X.-H. Zhou, C. Chen, H.-P. Xiao, Y.-Z. Li, J.-L. Zuo and X.-Z. You, *Cryst. Growth Des.*, 2009, **9**, 1041–1053.

3 N. T. Nguyen, H. Furukawa, F. Gandara, H. T. Nguyen, K. E. Cordova and O. M. Yaghi, *Angew. Chem., Int. Ed.*, 2014, **53**, 10645–10648.

4 G. Resnati, E. Boldyreva, P. Bombicz and M. Kawano, *IUCrJ*, 2015, **2**, 675–690.

5 Z.-L. Wang, W.-H. Fang and G.-Y. Yang, *Chem. Commun.*, 2010, **46**, 8216–8218.

6 E. Klontzas, A. Mavrandonakis, E. Tylianakis and G. E. Froudakis, *Nano Lett.*, 2008, **8**, 1572–1576.

7 S. S. Kaye, A. Dailly, O. M. Yaghi and J. R. Long, *J. Am. Chem. Soc.*, 2007, **129**, 14176–14177.

8 I. Senkovska, F. Hoffmann, M. Fröba, J. Getzschmann, W. Böhlmann and S. Kaskel, *Microporous Mesoporous Mater.*, 2009, **122**, 93–98.

9 Y. Li, C. Xiao, S. Li, Q. Chen, B. Li, Q. Liao and J. Niu, *J. Solid State Chem.*, 2013, **200**, 251–257.

10 Y. Zhao, N. Kornienko, Z. Liu, C. Zhu, S. Asahina, T.-R. Kuo, W. Bao, C. Xie, A. Hexemer and O. Terasaki, *J. Am. Chem. Soc.*, 2015, **137**, 2199–2202.

11 A. Chen and S. Chatterjee, *Chem. Soc. Rev.*, 2013, **42**, 5425–5438.

12 W. Liu and X.-B. Yin, *TrAC, Trends Anal. Chem.*, 2016, **75**, 86–96.

13 A. Morozan and F. Jaouen, *Energy Environ. Sci.*, 2012, **5**, 9269–9290.

14 L. Liu, Y. Zhou, S. Liu and M. Xu, *ChemElectroChem*, 2017, **5**, 6–19.

15 A. Karmakar, P. Samanta, A. V. Desai and S. K. Ghosh, *Acc. Chem. Res.*, 2017, **50**, 2457–2469.

16 E. Bakker, P. Bühlmann and E. Pretsch, *Chem. Rev.*, 1997, **97**, 3083–3132.

17 P. Bühlmann, E. Pretsch and E. Bakker, *Chem. Rev.*, 1998, **98**, 1593–1688.

18 M. Pawlak, E. Grygolowicz-Pawlak and E. Bakker, *Anal. Chem.*, 2010, **82**, 6887–6894.

19 W.-H. Li, K. Ding, H.-R. Tian, M.-S. Yao, B. Nath, W.-H. Deng, Y. Wang and G. Xu, *Adv. Funct. Mater.*, 2017, **27**, 1702067.

20 M. Sohail, R. De Marco, Z. Jarolímová, M. Pawlak, E. Bakker, N. He, R.-M. Latonen, T. Lindfors and J. Bobacka, *Langmuir*, 2015, **31**, 10599–10609.

21 W. P. Lustig, S. Mukherjee, N. D. Rudd, A. V. Desai, J. Li and S. K. Ghosh, *Chem. Soc. Rev.*, 2017, **46**, 3242–3285.

22 X.-Y. Dong, R. Wang, J.-Z. Wang, S.-Q. Zang and T. C. W. Mak, *J. Mater. Chem. A*, 2015, **3**, 641–647.

23 R. W. Huang, Y. S. Wei, X. Y. Dong, X. H. Wu, C. X. Du, S. Q. Zang and T. C. W. Mak, *Nat. Chem.*, 2017, **9**, 689–697.

24 Z. Hu, B. J. Deibert and J. Li, *Chem. Soc. Rev.*, 2014, **43**, 5815–5840.

25 R. Wang, X.-Y. Dong, H. Xu, R.-B. Pei, M.-L. Ma, S.-Q. Zang, H.-W. Hou and T. C. W. Mak, *Chem. Commun.*, 2014, **50**, 9153–9156.

26 P. Ramaswamy, N. E. Wong, B. S. Gelfand and G. K. H. Shimizu, *J. Am. Chem. Soc.*, 2015, **137**, 7640–7643.

27 S. K. Mehta, K. Singh, A. Umar, G. R. Chaudhary and S. Singh, *Electrochim. Acta*, 2012, **69**, 128–133.

28 M. M. Rahman, V. G. Alfonso, F. Fabregat-Santiago, J. Bisquert, A. M. Asiri, A. A. Alshehri and H. A. Albar, *Microchim. Acta*, 2017, **184**, 2123–2129.

29 C. A. Reilly and S. D. Aust, *Chem. Res. Toxicol.*, 1997, **10**, 328–334.

30 S. Garrod, M. E. Bollard, A. W. Nicholls, S. C. Connor, J. Connelly, J. K. Nicholson and E. Holmes, *Chem. Res. Toxicol.*, 2005, **18**, 115–122.

31 J.-A. Oh and H.-S. Shin, *J. Chromatogr. A*, 2015, **1395**, 73–78.

32 Z. Xu, M. Pang, C. Li and B. Zhu, *Luminescence*, 2017, **32**, 466–470.

33 A. D. Arulraj, M. Vijayan and V. S. Vasantha, *Spectrochim. Acta, Part A*, 2015, **148**, 355–361.

34 H. Hamidi, S. Bozorgzadeh and B. Haghighi, *Microchim. Acta*, 2017, **184**, 4537–4543.

35 Y. Zhou, J. Li, S. Wang, J. Zhang and Z. Kang, *J. Mater. Sci.*, 2017, **52**, 12089–12097.

36 Y.-Y. Zheng, C.-X. Li, X.-T. Ding, Q. Yang, Y.-M. Qi, H.-M. Zhang and L.-T. Qu, *Chin. Chem. Lett.*, 2017, **28**, 1473–1478.

37 D. Brondani, E. Zapp, R. da Silva Heying, B. de Souza and I. C. Vieira, *Electroanalysis*, 2017, **29**, 2810–2817.

38 L. Wang, Q. Teng, X. Sun, Y. Chen, Y. Wang, H. Wang and Y. Zhang, *J. Colloid Interface Sci.*, 2018, **512**, 127–133.

39 Y. Wang, L. Wang, W. Huang, T. Zhang, X. Hu, J. A. Perman and S. Ma, *J. Mater. Sci.*, 2017, **5**, 8385–8393.

40 Y. Sun, Y. Li, N. Wang, Q. Q. Xu, L. Xu and M. Lin, *Electroanalysis*, 2018, **30**, 474–478.

41 L. Yang, C. Xu, W. Ye and W. Liu, *Sens. Actuators, B*, 2015, **215**, 489–496.

42 M. D. García, M. L. Marcos and J. G. Velasco, *Electroanalysis*, 1996, **8**, 267–273.

43 P. Kumar, A. Deep and K.-H. Kim, *TrAC, Trends Anal. Chem.*, 2015, **73**, 39–53.

44 M. A. Abdel Rahim, R. M. Abdel Hameed and M. W. Khalil, *J. Power Sources*, 2004, **134**, 160–169.

45 A. V. Tripković, K. D. Popović, J. D. Momčilović and D. M. Dražić, *J. Electroanal. Chem.*, 1998, **448**, 173–181.

46 L. Aldous and R. G. Compton, *Phys. Chem. Chem. Phys.*, 2011, **13**, 5279–5287.